



HAL
open science

Improving Accuracy and Integrity with a Probabilistic Urban Trench Modeling

David Bétaille, François Peyret, Miguel Ortiz, Stéphane Miquel, Frédéric Godan

► **To cite this version:**

David Bétaille, François Peyret, Miguel Ortiz, Stéphane Miquel, Frédéric Godan. Improving Accuracy and Integrity with a Probabilistic Urban Trench Modeling. *Navigation*, 2016, 63 (3), pp.283-294. 10.1002/navi.145 . hal-04462720

HAL Id: hal-04462720

<https://univ-eiffel.hal.science/hal-04462720>

Submitted on 16 Feb 2024

HAL is a multi-disciplinary open access archive for the deposit and dissemination of scientific research documents, whether they are published or not. The documents may come from teaching and research institutions in France or abroad, or from public or private research centers.

L'archive ouverte pluridisciplinaire **HAL**, est destinée au dépôt et à la diffusion de documents scientifiques de niveau recherche, publiés ou non, émanant des établissements d'enseignement et de recherche français ou étrangers, des laboratoires publics ou privés.

Improving Accuracy and Integrity with a Probabilistic Urban Trench Modeling

D. BÉTAILLE, F. PEYRET, and M. ORTIZ
IFSTTAR, Grenoble, France

S. MIQUEL and F. GODAN
SCM SA, Paris, France

Received March 2015; Revised January 2016

ABSTRACT: *GNSS localization in an urban environment remains a key issue that must be solved in order to enable innovative driver assistance systems or cooperative applications. This issue exists not only in terms of accuracy but also in terms of integrity. Actually, one aims at reducing as much as possible the error mainly due to multipath on buildings and provide in the mean time a certain guarantee on the user position exactness. This article shows how a simple geometric modeling, named 'Urban Trench', of the city environment can improve significantly the positioning accuracy. Authors also propose an algorithm for computing an urban trench protection level, with a much higher reliability compared to conventional protection level whose open sky assumption is violated. Experimental results are given in the cities of Nantes, Paris, and Toulouse, France. Copyright © 2016 Institute of Navigation*

INTRODUCTION

While Intelligent Transportation Systems (ITS) concentrate most applications in dense city areas, urban positioning using GNSS is still challenging because of multipath. As concerns personal car driving, the emergence of new applications like lane change control, or lane keeping systems, or cooperative driving assistance, is still missing lane-level accuracy. Even if advanced localization systems will make use of camera vision and lidar, as additional exteroceptive devices, and also fuse these with proprioceptive sensors, reliable GNSS solutions are not only very useful but considered as mandatory for initialization and re-initialization of such a multisensory process. Reliability here means not only accuracy but also availability and integrity. Urban canyons prevent open sky visibility and also cause signal reflection and diffraction, prone to introducing into the receiver position solution additional traveled distances to satellites, and finally generating severe positioning deviation, up to several tenths of meters in certain critical situations [1].

Several directions of research exist

- at the GNSS hardware level, with specific antenna devices, and with multipath rejecting tracking

loops: a limited success has been achieved, in particular as concerns low-cost and high-sensitivity GNSS equipment, which is actually used in most car and individual positioning;

- at the navigation software level, using, e.g., signal-to-noise ratio measurement selection and weighting, or solution constraints like the road surface, or, more recently, 3D digital city models, those being used in algorithms capable of separating the satellites in line-of-sight (LOS) from those in non-line-of-sight (NLOS): the latter of these cause the largest range and position errors. [2] gives a comprehensive review of the state of the art.

The research investigations reported in this article use 3D modeling and have been carried out in the frame of a French national project called Inturb (an acronym between integrity and urban positioning), funded by the Ministry responsible for transport in France, DGITM (general directorate for infrastructure, transport, and the sea). So far, the project has had two phases. During the first phase, a simple 3D geometric city modeling, called 'Urban Trench', has been proposed and engineered manually on a data set collected in three different cities: Nantes, Paris, and Toulouse. Positioning improvement in terms of accuracy was quantified where the model could be applied. In the second phase, this modeling has been automated, based on the standard national BD Topo

1 © map database, with again promising results, along
 2 with an applicability generalized everywhere. The
 3 geometric modeling will be presented in the first
 4 section.

5 In order to take into account the uncertainties of
 6 both the vehicle positioning and the building
 7 geometry, the deterministic law previously used
 8 has been modified in the most recent investigations
 9 carried out. The summarized idea is this: instead of
 10 considering that all satellites above critical ele-
 11 vation are in LOS, a percentage of these will be
 12 considered as NLOS. A computation of an urban
 13 integrity indicator is proposed on this probabilistic
 14 basis. The probabilistic modeling will be presented
 15 in the second section. Experimental results in
 16 terms of integrity improvement will be shown in
 17 the third section, followed by conclusions and
 18 perspectives.

21 GEOMETRIC MODELING

22 The geometric modeling of cities makes possible
 23 the separation of satellites in line-of-sight (LOS)
 24 from those in non-line-of-sight (NLOS). This has
 25 been demonstrated by several research groups [3–
 26 6], including the authors' group [7–9]. LOS-only
 27 methods consist in excluding from the positioning
 28 solver set the NLOS satellites once detected: [3–5,
 29 7, 8]. Nevertheless, a correction of the NLOS
 30 pseudorange measurements is possible, on the basis
 31 of geometric considerations, and also computed and
 32 applied in the positioning solution: [6, 9].

33 Except [9], the state-of-the-art relies on a relatively
 34 detailed modeling, where the critical elevation due to
 35 a building in a given satellite azimuth is specifically
 36 computed, either directly by ray-tracing in the city
 37 model itself, or by comparison to building boundaries
 38 in azimuth-elevation diagrams stored everywhere in
 39 the concerned areas by grid steps of, e.g., 2 m.

40 Whereas, most 'skyplot' diagrams show a detailed
 41 LOS/NLOS boundary, e.g., with one degree resolution,
 42 our approach is simpler. The skyplot is oriented along
 43 the street direction, and the street geometry is
 44 averaged, making only two left and right boundaries
 45 available for satellite selection. In a few words, our
 46 building boundary, or 'mask of visibility', looks like a
 47 F1 rugby ball (Figure 1), because of our so-called 'Urban
 48 Trench' modeling.

49 The parameters of the model are, per arc segment,

- 50 • its id;
- 51 • its direction angle;
- 52 • its point coordinates;
- 53 • its neighbor's id list (for a fast map-matching
 54 process);
- 55 • the average distance to the buildings situated at
 56 its left
- 57 • and their average height (W_1, H_1);

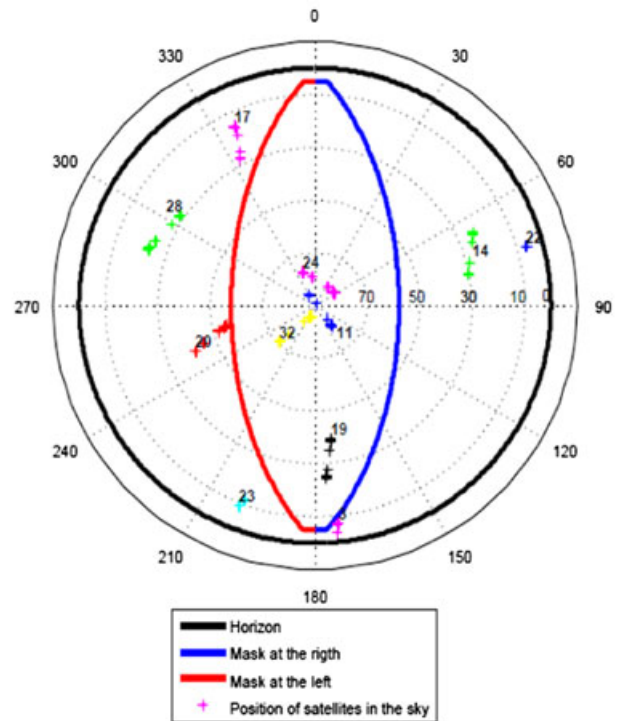
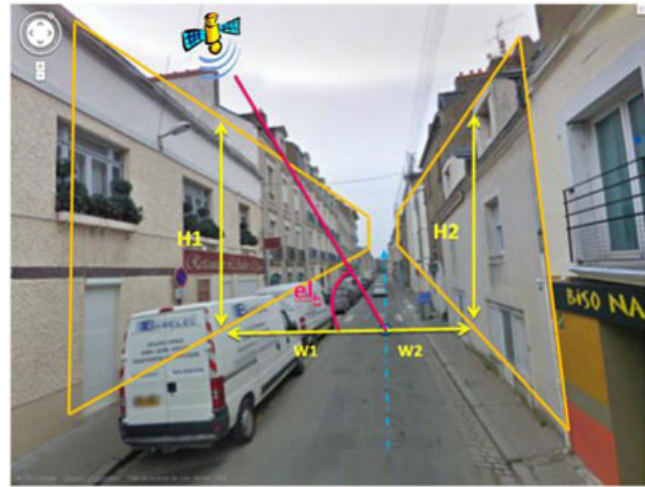


Fig. 1—Overview of the characteristics of a street in Nantes, typical of an Urban Trench, and the corresponding road and building BD Topo © layers and obtained mask of visibility. [Color figure can be viewed in the online issue, which is available at wileyonlinelibrary.com and www.ion.org]

- the average distance to the buildings situated at its right
- and their average height (W_2, H_2).

The width and height parameters mix road and building layers of standard databases, here BD Topo ®. Specific programming has been made to enable the automatic computation of $W_1, H_1, W_2,$ and H_2 . All geometric data in BD Topo ® are given with 1dm resolution, and their exactness is of the order of magnitude of meter. In our approach, the building parameters are averaged per arc segment, whose length is typically of a few tens of meters.

For a satellite situated on the left side, the critical elevation above that one reflection occurs is given by

$$el_{01} = \arctg \left| \frac{H_1}{W_1} \sin(\beta) \right| \quad (1)$$

where β measures the angle difference between the satellite azimuth and the street direction.

We assume a maximum of two specular reflections. A similar formula can be obtained for consecutive reflections on both opposite sides of the street. These reflections lead to an error that is added to the pseudorange of the affected satellites: the additional distance. From the city geometric modeling and the satellites position, additional distances m_1 and m_2 are computed as follows:

$$m_1 = |2W_2 \cos(el) \sin(\beta)| \quad (2)$$

where el denotes the satellite elevation angle.

T1T2 Tables 1 and 2 give respectively the critical elevations and the additional distances for 1 and 2 reflections.

The main advantage of this model is structural: it actually matches the information structure of

Table 1—Critical elevations of transition LOS to NLOS one reflection, and transition NLOS one to two reflections. el_{01} defines the critical elevation angle separating signals with 0 and 1 reflection. el_{12} defines the critical elevation angle separating signals with one and two reflections

Critical elevation angle	
Left side	Right side
$el_{01} = \arctg \left \frac{H_1}{W_1} \sin(\beta) \right $	$el_{01} = \arctg \left \frac{H_2}{W_2} \sin(\beta) \right $
$el_{12} = \arctg \left \frac{H_1}{W_1 + 2W_2} \sin(\beta) \right $	$el_{12} = \arctg \left \frac{H_2}{W_2 + 2W_1} \sin(\beta) \right $

Table 2—Corresponding additional distances

Nb of reflections	Additional distance	
	Left side	Right side
0	$m_0 = 0$	
1	$m_1 = 2W_2 \cos(el) \sin(\beta) $	$m_1 = 2W_1 \cos(el) \sin(\beta) $
2	$m_2 = 2(W_1 + W_2) \cos(el) \sin(\beta) $	

geographic data stored in car navigation systems or handheld navigation devices. As a consequence, we estimate that the data storage capacity required for our Urban Trench Method to run is one order of magnitude lower than that necessary for detailed building critical elevation modeling.

PROBABILISTIC MODELING

Whereas, the initial approach was totally deterministic, we will now introduce probabilistic modeling. The motivation for this new modeling is the following: along the street arc segments, if the heights and widths are not unified, the model is not perfectly applicable and the results are not optimal. The same happens if the database is not up to date. This is why a purely deterministic model cannot apply and motivates a probabilistic approach.

This analysis considers the distribution of the range errors. These errors are the differences between the geometric distances and the measured pseudoranges, these being corrected by Hopfield tropospheric and broadcast ionospheric terms, satellite clock terms, and receiver clock term (by means of the highest satellite per epoch, assumed multipath free). The geometric distances are based on the ground truth obtained using IFSTTAR VERT, our Vehicle for Experimental Research on Trajectories [10], which embeds an IXSea inertial unit and a dual-frequency Novatel GPS receiver.

The distribution of the range errors, when we consider a large data set, is Gaussian in an open area, but it shows a queue of positive values in the urban environment. On data subsets, we have sought to match a multi-modal Gaussian law to this distribution (see Figure 2), whose parameters depend on the street geometry, and on the azimuth and elevation of the satellites considered.

The analysis has been conducted using mainly Paris data previously logged. In streets with the same geometric configuration (i.e., similar width and height), the skyplot is cut into strips of equal size, each corresponding to an area between two elevations, these being modulated by the azimuth relative to the street direction, in order to take into account the Urban Trench geometry. This identifies satellites with equivalent visibility with respect to the local environment. The comparison of the range errors with respect to the additional distances performed in the case of multipath shows that part of the satellites in a strip do not conform to the model. Where we expect one reflection, e.g., in a strip, a certain percentage will actually experience two reflections (or no reflection). This has been probabilistically modeled. Thus, the uncertainty in the number of reflections on buildings is considered as identical for all satellites in a given strip.

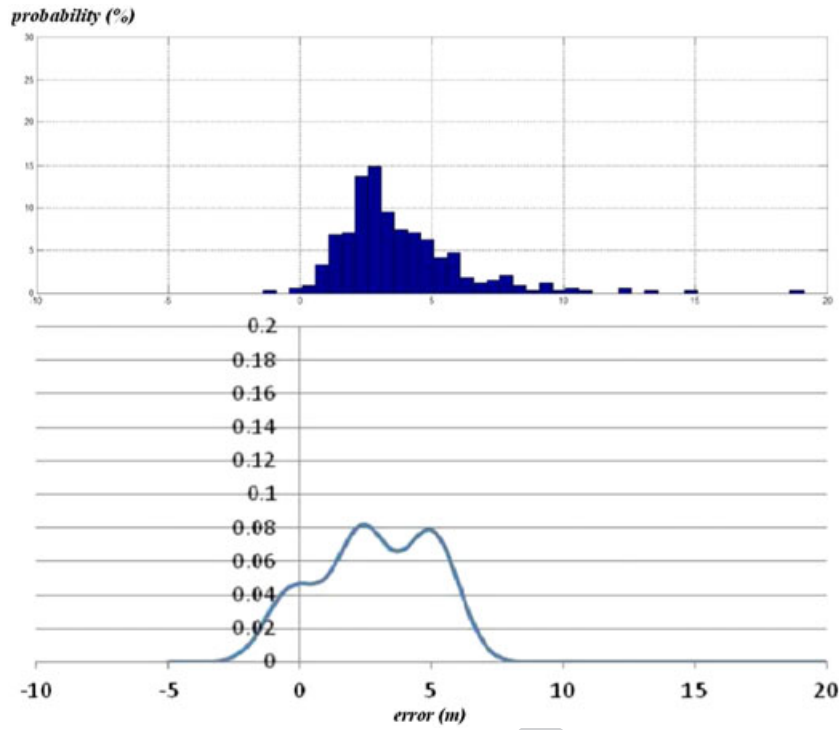


Fig. 2–Top: subset of range errors, for a given geometric configuration (narrow street and high buildings) and satellites relatively low in elevation, respective to the buildings around. Bottom: corresponding multimodal modeling. [Color figure can be viewed in the online issue, which is available at wileyonlinelibrary.com and www.ion.org]

Let P_0 , P_1 , and P_2 be the probabilities to have 0, 1, and 2 reflections with $P_0 + P_1 + P_2 = 1$. From the measurements collected previously in Paris, a model is built. The probabilities are expressed as a function

of the elevation of the satellite with respect to the critical elevations, el_{01} and el_{12} , these depending on the geometric modeling locally and the azimuth difference β (Figure 3). **F3**

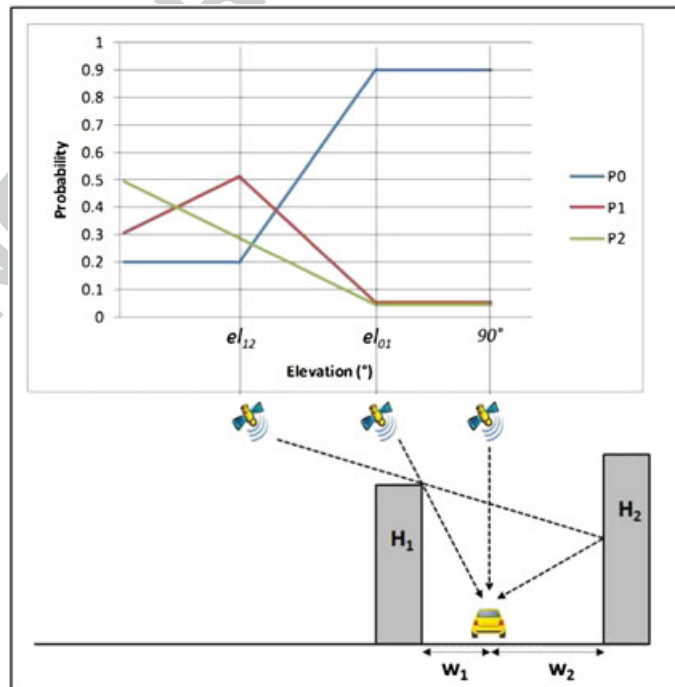


Fig. 3–Model of probabilities P_0 , P_1 , and P_2 . [Color figure can be viewed in the online issue, which is available at wileyonlinelibrary.com and www.ion.org]

1 A multimodal Gaussian law cannot let an explicit
 2 computation of the navigation solution and its pro-
 3 tection level be made. Only Monte Carlo techniques
 4 could approximate such distribution. With this model,
 5 we have simplified the distribution, considering only
 6 its modes. Finally, the error law of the signal is a
 7 discrete probability distribution formed of three
 8 additional distances associated to their probability. A
 9 combinatory approach, instead of, e.g., a particle filter,
 10 can then be used.

11 The additional distances m_0 , m_1 , or m_2 are
 12 subtracted from the pseudoranges. In a given epoch, n
 13 satellites are tracked. Thus, 3^n positions of the receiver
 14 are computed with a least squares solver, combining
 15 the three different possible cases of reflection, each
 16 associated with a probability $P = P_0P_1P_2$.

17 PROTECTION LEVEL DERIVATION

18 The expectation of this ‘cloud’ of positions gives the
 19 corrected position of the receiver. The major axis of the
 20 ellipsoid that encompasses all positions is multiplied
 21 by K to obtain the three-dimensional Protection Level
 22 (3DPL), this K factor being obtained as usual in the
 23 inverse χ^2 statistic table for a specified probability
 24 P_{md} of missed detection and for the considered
 25 dimensions (here three). Note that, for conservative
 26 purpose, K is often fixed to four dimensions, e.g., in
 27 [11]: $K(P_{md}, 4) = 6.18$ for $P_{md} = 10^{-7}$. The weighting
 28 vector and the position expectation (i.e., the weighted
 29 average of the 3^n positions $[X\ Y\ Z]$ combined, indexed
 30 from the 1st to the 3^n th) are, respectively,

$$31 \quad w = \begin{bmatrix} P_{1^{st}} \\ \dots \\ P_{3^{nth}} \end{bmatrix} \quad (3)$$

$$32 \quad \bar{p} = w^t \begin{bmatrix} [XYZ]_{1^{st}} \\ \dots \\ [XYZ]_{3^{nth}} \end{bmatrix} \quad (4)$$

33 The position covariance matrix is

$$34 \quad \Sigma = \begin{bmatrix} [XYZ]_{1^{st}} - \bar{p} & \dots & [XYZ]_{3^{nth}} - \bar{p} \\ \dots & \dots & \dots \\ [XYZ]_{3^{nth}} - \bar{p} & \dots & \dots \end{bmatrix} \begin{bmatrix} P_{1^{st}} & 0 & 0 \\ 0 & \dots & 0 \\ 0 & 0 & P_{3^{nth}} \end{bmatrix} \begin{bmatrix} [XYZ]_{1^{st}} - \bar{p} \\ \dots \\ [XYZ]_{3^{nth}} - \bar{p} \end{bmatrix} \quad (5)$$

35 This matrix has the following form:

$$36 \quad \Sigma = \begin{bmatrix} \sigma_X^2 & \sigma_{XY} & \sigma_{XZ} \\ \sigma_{XY} & \sigma_Y^2 & \sigma_{YZ} \\ \sigma_{XZ} & \sigma_{YZ} & \sigma_Z^2 \end{bmatrix} \quad (6)$$

37 from which the 3D protection level of the Urban
 38 Trench Probabilistic Method is finally derived:

$$39 \quad 3DPL_{Utpm} = K(P_{md}) * \sqrt{\max(\text{eigenvalue}(\Sigma))} \quad (7)$$

40 Similarly, but without any use of the local 3D city
 41 model, a standard 3D protection level can be

42 computed: this is based on the XYZ components
 43 (excluding the clock term component) of the H matrix
 44 [12] that is used in the ordinary epoch per epoch least
 45 squares solution, and gathers all satellites in view,
 46 irrespectively of their relative position to buildings.
 47 This conventional positioning uses all satellite
 48 pseudoranges, with no particular weighting, neither
 49 fault detection and exclusion nor filtering.

50 The standard 3DPL assumes open sky visibility,
 51 like civil aviation does [11]. The standard deviation
 52 of the user equivalent range error (UERE) is a priori
 53 unknown and can be based on the pseudorange
 54 least-squares residuals ε .

$$55 \quad 3DPL_{std} = K(P_{md}) * \sqrt{\max(\text{eigenvalue}(H^t H)) * \sigma_{uere}} \quad (8)$$

56 A way to estimate σ_{uere} is

$$57 \quad \sigma_{uere} \approx \|\varepsilon\| / \sqrt{n - 4} \quad (9)$$

58 Because the vertical dimension is not necessary for
 59 most ITS applications, it is suggested to also compute
 60 protection levels in 2D, leading to the commonly used
 61 HPL. The HPL for the Urban Trench Probabilistic
 62 Method is derived after a projection of the point cloud
 63 in the Earth local tangent frame, which gives East,
 64 North, and Up coordinates (ENU) instead of geocentric
 65 ones (XYZ). Only the EN sub-matrix is considered:

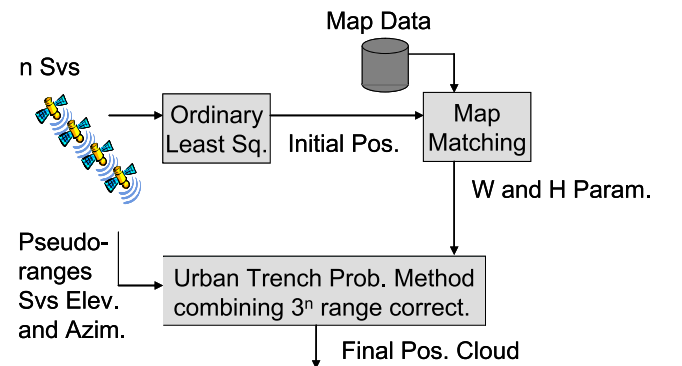
$$66 \quad \Sigma_{EN} = \begin{bmatrix} \sigma_E^2 & \sigma_{EN} \\ \sigma_{EN} & \sigma_N^2 \end{bmatrix} \quad (10)$$

67 from which the HPL of the Urban Trench
 68 Probabilistic Method is similarly derived:

$$69 \quad HPL_{Utpm} = K(P_{md}) * \sqrt{\max(\text{eigenvalue}(\Sigma_{EN}))} \quad (11)$$

70 Lastly, the standard HPL is computed after
 71 applying onto H the XYZ-to-ENU rotation matrix,
 72 giving G, whose EN components are considered:

$$73 \quad HPL_{std} = K(P_{md}) * \sqrt{\max(\text{eigenvalue}(G_{EN}^t G_{EN})) * \sigma_{uere}} \quad (12)$$



74 Fig. 4—UTPM flowchart. [Color figure can be viewed in the online
 75 issue, which is available at wileyonlinelibrary.com and www.ion.org]

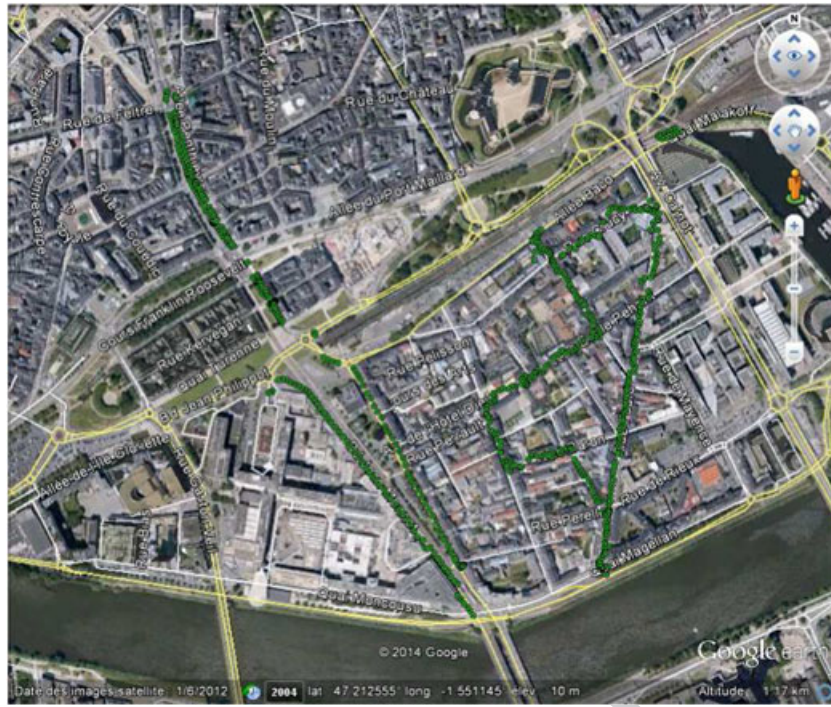


Fig. 5—Overview of Nantes city center test site. [Color figure can be viewed in the online issue, which is available at wileyonlinelibrary.com and www.ion.org]

Table 3—Positioning error statistics in 3D: the 5th, median, and 95th percentiles of the 3D position error are given, for both conventional with all satellites in view and Urban Trench probabilistic methods

3D error with all satellites (m)			3D error with UTPM (m)		
5th percentile	Median	95th percentile	5th percentile	Median	95th percentile
2.4	8.2	62.9	3.0	5.9	18.1

PROCESS OVERVIEW

Starting from an ordinary least squares solution, a map-matching is made in order to determine the local arc segment ID and its geometry. Using the identified geometric parameters, the UTPM is applied, and the initial solution is refined (Figure 4). There is actually no particle filter in this process, whereas this option was already investigated by the authors [13] with a map where several segments figure out several possible lateral positions in the street (i.e., different lanes or sidewalks).

PRELIMINARY RESULTS

To validate the Urban Trench Probabilistic Method, preliminary results are obtained from measurements in Nantes. The receiver was a Ublox LEA-6T, a typical OEM equipment used in car navigation systems. Its measurement update rate is 5 Hz. The test took about 18 min for 5,417 epochs measured. The UTPM is applied on part of these epochs (3,321 or 11 min), those

where the buildings around are high enough, i.e., 2.5 m above the antenna, and where at least five satellites are tracked (LOS or NLOS): this last condition causes several epochs with four satellites – for which the

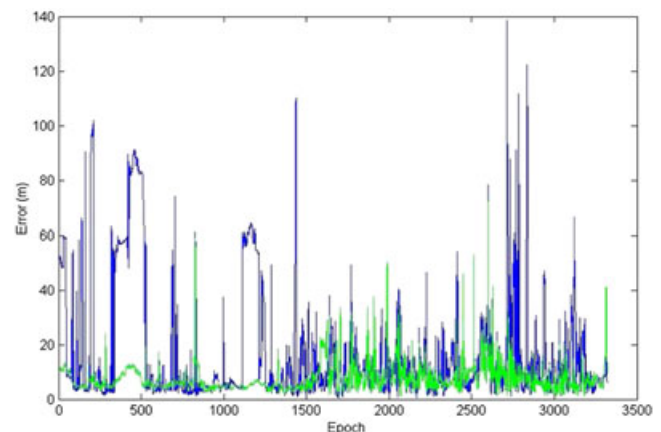


Fig. 6—Positioning error with all satellites (blue) and with the Urban Trench Probabilistic Method (green). [Color figure can be viewed in the online issue, which is available at wileyonlinelibrary.com and www.ion.org]

Table 4—3D Protection Level statistics: 5th, median and 95th percentiles of the 3DPL, for both methods. Nb of MI

Standard 3D protection level (m)			UTPM 3D protection level (m)		
5th percentile	Median	95th percentile	5th percentile	Median	95th percentile
7.2	25.9	140.9	57.9	88.2	162.6
Number of MI: 185			Number of MI: 1		

conventional positioning method operates, but not the PL derivation – to be removed. In this data set, five epochs are concerned. The ground truth was provided by the VERT. Figure 5 shows an overview of the epochs and streets concerned.

The median of the positioning error, in 3D, is improved from 8.2m when using all satellites to 5.9m when using the UTPM, which makes an

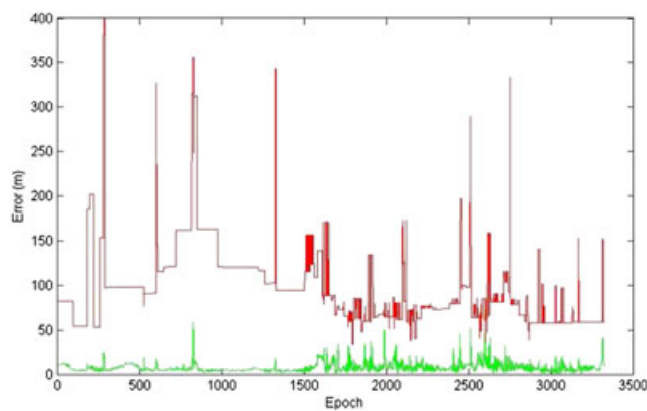


Fig. 7—Positioning error with the Urban Trench Probabilistic Method (green) and 3DPL (red). [Color figure can be viewed in the online issue, which is available at wileyonlinelibrary.com and www.ion.org]

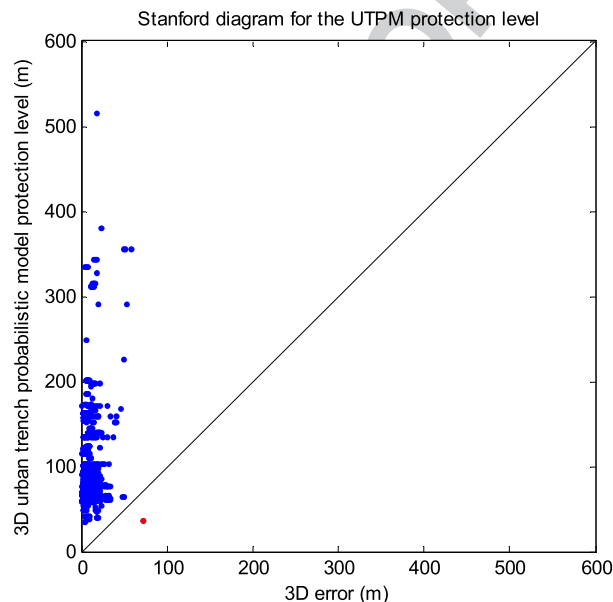


Fig. 8—Stanford diagram for UTPM protection level. [Color figure can be viewed in the online issue, which is available at wileyonlinelibrary.com and www.ion.org]

improvement of near 30% (see Table 3). A time series of the 3D error of both solutions is displayed in Figure 6. These results are close to those already obtained in Nantes (but also in Paris and Toulouse) with the Urban Trench deterministic model [14]. Note that in the first half of the test (West side), one travels in large boulevards, before entering narrower streets in the second half (East side). Errors are larger (and dramatically reduced using our geometric model) in large streets, typically Haussmann style-like in Paris.

The median of the 3DPL is 88.2 m (see Table 4). Only one solution (one epoch) is not actually protected among all 3DPL solutions (see Figure 7, and Stanford diagram Figure 8). The reason why this occurred at that epoch has not been investigated (see conclusions and perspectives). For the same data set, the standard protection level in 3D, with a median of 25.9m (by fixing the standard deviation of the range errors σ_{uere} with Equation (9) by means of the residuals), would give 185 Misleading Information (MI) epochs (see Stanford diagram Figure 9).

Preliminary results have shown that a significant improvement of the accuracy is still obtained. In the

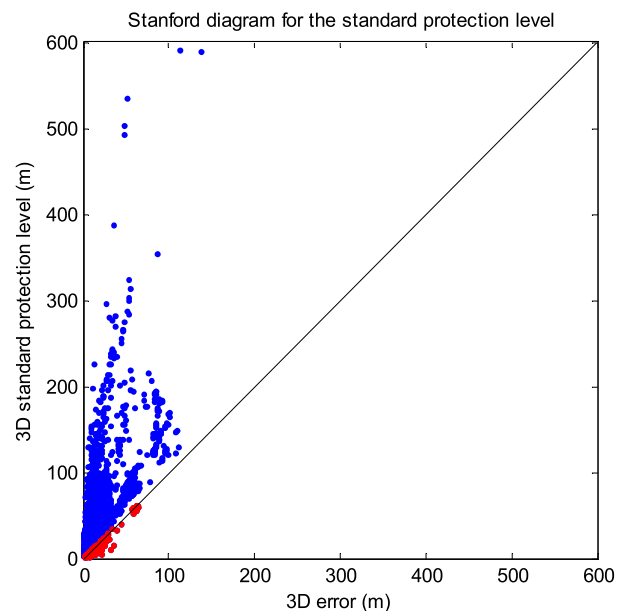


Fig. 9—Stanford diagram for standard protection level. Note: in the sequel of this article, complementary results are given in 3D and last in 2D. Tables, statistics (5th, median and 95th percentiles of errors and protection levels), and diagrams are presented, similarly as those already presented in Tables 3 and 4 and Figs. 8 and 9. [Color figure can be viewed in the online issue, which is available at wileyonlinelibrary.com and www.ion.org]

Table 5—Position error statistics in 3D for both methods

3D error with all satellites (m)			3D error with UTPM (m)		
5th percentile	Median	95th percentile	5th percentile	Median	95th percentile
3.3	23.4	87.3	3.0	10.7	47.9

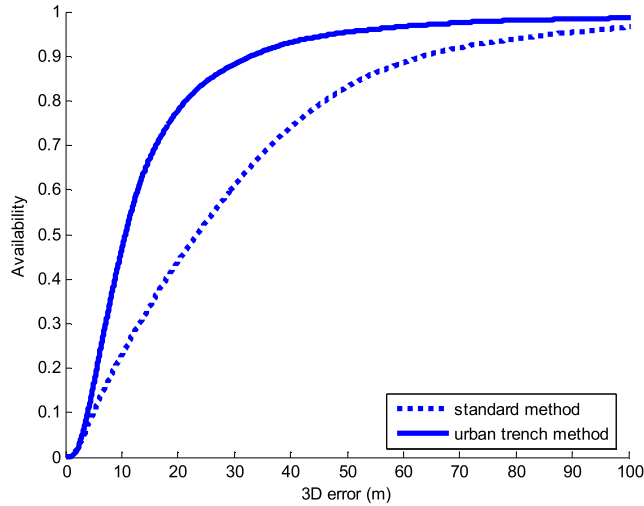


Fig. 10—Cumulative distribution function of the error, in 3D, for both standard and Urban Trench Methods. [Color figure can be viewed in the online issue, which is available at wileyonlinelibrary.com and www.ion.org]

mean time, a statistical indicator is achieved by computing the bounding ellipsoid of the solutions of the above combinations. The probabilistic Urban Trench method proposed gives a protection level that matches much better the true positioning error than the standard of civil aviation because local perturbations in signal propagation are taken into account.

COMPLEMENTARY RESULTS IN 3D

To complete the preliminary results, this section gathers the results obtained in Nantes (reported in the previous section) with those obtained in Paris and Toulouse during Phase 1, and also with those obtained in Nantes once again during Phase 2, with a new data collection.

Table 5 summarizes the results in terms of 3D positioning error, with the Urban Trench

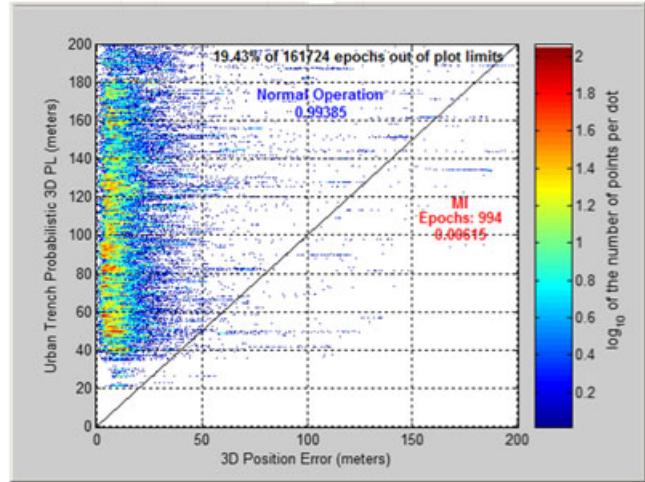


Fig. 11—Stanford diagram for UTPM 3DPL. [Color figure can be viewed in the online issue, which is available at wileyonlinelibrary.com and www.ion.org]

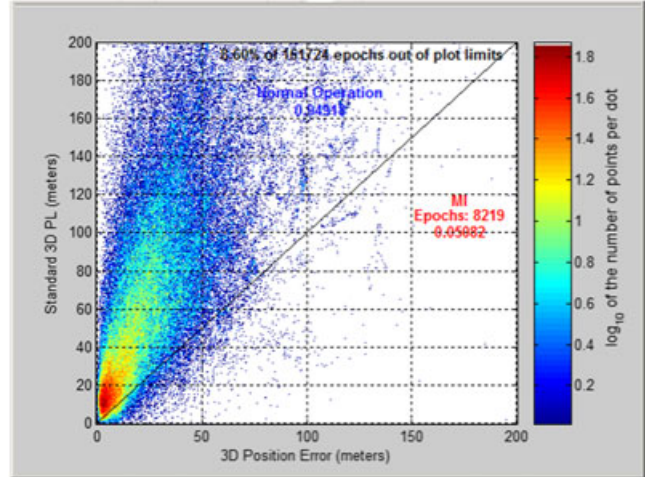


Fig. 12—Stanford diagram for standard 3DPL. [Color figure can be viewed in the online issue, which is available at wileyonlinelibrary.com and www.ion.org]

Table 6—3DPL statistics for both methods. Nb of MI. Note: The conventional positioning method operates for 163,503 epochs, versus 161,724 for the PL derivation as well as for the UTPM, the difference (1,779 epochs, i.e., 1%) being epochs with only four satellites

Standard 3D protection level (m)			UTPM 3D protection level (m)		
5th percentile	Median	95th percentile	5th percentile	Median	95th percentile
10.0	64.5	258.3	47.2	119.9	360.2
Number of MI: 8,219			Number of MI: 994		

Table 7—Position error statistics in 2D for both methods

Horizontal error with all satellites (m)			Horizontal error with UTPM (m)		
5th percentile	Median	95th percentile	5th percentile	Median	95th percentile
1.3	10.2	42.8	1.3	6.2	27.8



Table 8—HPL statistics for both methods. Nb of MI

Standard HPL (m)			UTPM HPL (m)		
5th percentile	Median	95th percentile	5th percentile	Median	95th percentile
5.7	38.2	152.7	32.9	87.0	222.0
Number of MI: 4,838			Number of MI: 635		

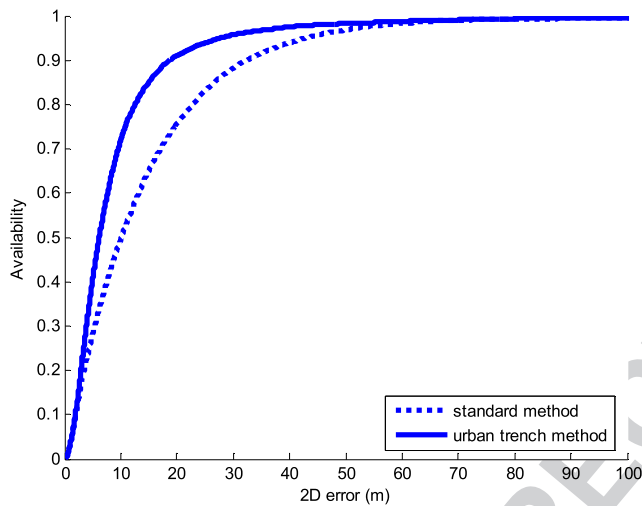


Fig. 13—Cumulative distribution function of the error, in 2D, for both standard and Urban Trench Methods. [Color figure can be viewed in the online issue, which is available at wileyonlinelibrary.com and www.ion.org]

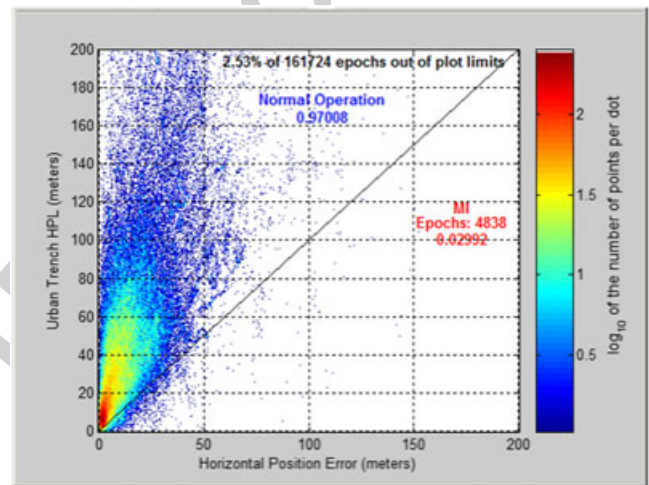


Fig. 15—Stanford diagram for standard HPL. [Color figure can be viewed in the online issue, which is available at wileyonlinelibrary.com and www.ion.org]

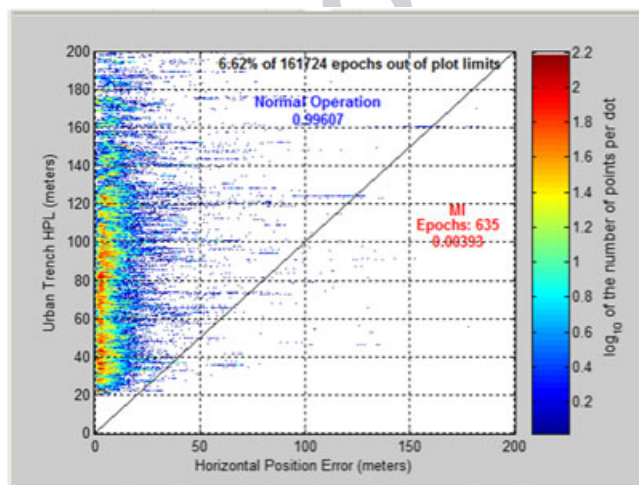


Fig. 14—Stanford diagram for UTPM HPL. [Color figure can be viewed in the online issue, which is available at wileyonlinelibrary.com and www.ion.org]

deterministic model. The receiver is the same Ublox LEA-6T, with a measurement update rate of 5 Hz. The total test duration is approximately 11½h, for 208,357 epochs measured. The UTPM is applied on part of these epochs (161,724 or near 9 h). The median of the positioning error, in 3D, is improved from 23.4 m to 10.7m with the UTPM, which makes an improvement of 54% (see Figure 10 and Table 5).

The median of the 3DPL is 119.9.m (see Table 6). A total of 994 solutions are not protected among all 3D UTPM solutions (MI). For the same data set, the standard protection level in 3D, with a median of 64.5 m (by fixing the standard deviation of the range errors σ_{uere} with Equation (9) by means of the residuals), gives 8,219 MI epochs (see Stanford diagram Figures 11 and 12).

RESULTS IN 2D

HPL results will be given before concluding. Tables 7 and 8 summarize the results considering

1
2
3
4
5
6
7
8
9
10
11
12
13
14
15
16
17
18
19
20
21
22
23
24
25
26
27
28
29
30
31
32
33
34
35
36
37
38
39
40
41
42
43
44
45
46
47
48
49
50
51
52
53
54
55
56
57
58
59
60
61

Table 9—3DPL statistics for both methods. Nb of MI

Standard 3D protection level (m) including a unique bias impact		UTPM 3D protection level (m)	
5th percentile	Median	5th percentile	95th percentile
15.0	95.7	119.9	360.2
Number of MI: 2,535		Number of MI: 994	

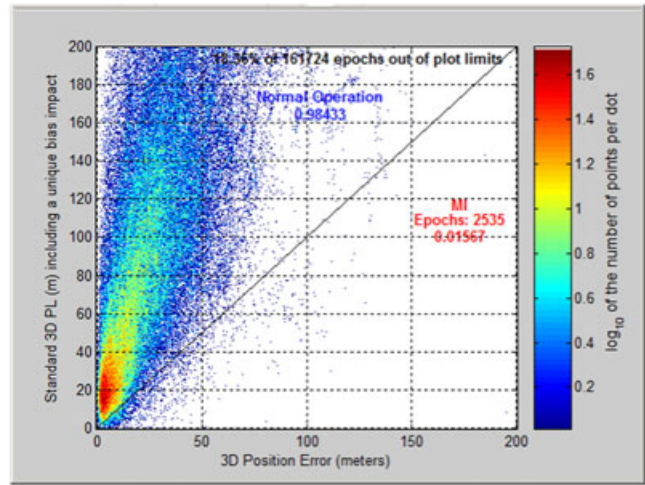


Fig. 16—Stanford diagram for standard 3DPL including a unique bias impact. [Color figure can be viewed in the online issue, which is available at wileyonlinelibrary.com and www.ion.org]

the horizontal dimension only, with 39% improvement of the plane median error, as shown on Figure 13 and Table 7.

The median of the HPL is 87.0m (see Table 8). A total of 635 solutions are not protected among all 2D UTPM solutions (MI). For the same data set, the standard protection level in 2D, with a median of only 38.2m (by fixing the standard deviation of the range errors σ_{uere} with Equation (9) by means of the residuals), gives 4,838 MI epochs (see Figures 14 and 15).

DISCUSSION

What is noticeable with UT protection levels, in 3D and in 2D, is that they are never very small, i.e., at the order of magnitude of the meter. On the contrary, they show a floor value of around 20m in our experiment. This is due to the fact the m_1 and m_2 are floored to 5 and 10m, respectively (see Table 2), which means that, if NLOS reflections are expected, they are assumed to impact the range measurements at a minimum level.

Obviously, UT protection levels are conservative as compared to the standard protection levels when applied to the context of this experiment. They much better match the expected MI.

The issue raised with estimating the standard deviation of the user equivalent range error σ_{uere} has been fixed using the residuals. These residuals, because they absorb part of the observation error, are only partially informative about large multipath effects in urban environments, which may be caused by NLOS satellites. These must be considered as biases.

The conventional PL derivation deals with the occurrence of a bias on a unique satellite at a time. In this section, we suggest to reconsider the

F13
F14
F15

62
63
64
65
66
67
68
69
70
71
72
73
74
75
76
77
78
79
80
81
82
83
84
85
86
87
88
89
90
91
92
93
94
95
96
97
98
99
100
101
102
103
104
105
106
107
108
109
110
111
112
113
114
115
116
117
118
119
120
121
122

Table 10—HPL statistics for both methods. Nb of MI

Standard HPL (m) including a unique bias impact			UTPM HPL (m)		
5th percentile	Median	95th percentile	5th percentile	Median	95th percentile
8.7	57.7	239.7	32.9	87.0	222.0
Number of MI: 1,445			Number of MI: 635		

computation of the standard protection levels including a bias term [15].

A conservative way to proceed is given by the addition in Equation (8) of the maximum impact of a bias expected from the examination of the residuals, leading to Equation (13):

$$3DPL_{std} = K(P_{md}) * \sqrt{\max(\text{eigenvalue}(H^+H))} * \sigma_{uere} + \max(\text{slope}_i) * \|\varepsilon\| \quad (13)$$

where

$$\text{slope}_i = \sqrt{\frac{H_{X,i}^{+2} + H_{Y,i}^{+2} + H_{Z,i}^{+2}}{(I + HH^+)_{i,i}}} \quad (14)$$

H^+ denotes the pseudo-inverse of H .

The same formulation in the EN local plane (instead of XYZ) applies for HPL.

In 3D, the statistics and Stanford diagram are the following (Table 9 and Figure 16), on our data set:

In 2D, the statistics and Stanford diagram are the following (Table 10 and Figure 17), on our data set:

Lastly, we have removed part of the data set that was logged in La Défense business center, whose skyscrapers do not match with the Urban Trench model. 11,166 epochs have been removed, over a total of 161,724. Only 325 MI remain.

What can be noticed with these last results is that the conventional protection levels, both in 3D and in 2D, still fail to encompass large positioning errors.

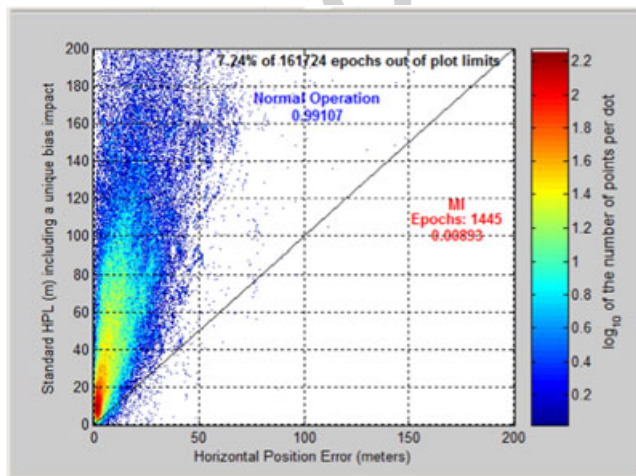


Fig. 17—Stanford diagram for standard HPL including a unique bias impact. [Color figure can be viewed in the online issue, which is available at wileyonlinelibrary.com and www.ion.org]

These, of course, occur because of NLOS satellites, which are numerous, in violation of the unique bias hypothesis usually formulated.

CONCLUSIONS AND PERSPECTIVES

To conclude, let us summarize and give a short description of the new and innovative aspects of this research work. The Urban Trench Probabilistic Method (UTPM) applies multipath specular assumption onto pseudorange measurements, considering local 3D map model, and, as the main contribution of this article, makes possible the computation of a protection level adapted to this environment and its modeling. Accuracy is improved: median 3D errors are typically cut in half.

Considering the results already obtained for a duration of approximately 9h, we claim that the UTPM guarantees a median 3D protection level on an order of magnitude of 100m in a dense urban environment, and an integrity risk of $6 \cdot 10^{-3}$ with a 10% confidence.

Since ground transportation does not use the vertical dimension, horizontal error improvement and protection level are of great interest. We have obtained a reduction of the 2D error close to 40%. The HPL has again an order of magnitude of 100m in median, and the integrity risk finally obtained is $4 \cdot 10^{-3}$ with a 10% confidence in 2D. This result is even better ($2 \cdot 10^{-3}$) if we remove from our data set the business center of Paris La Défense, duration 1/2h, where the Urban Trench Model does not properly apply. It is particularly noticeable that, at a similar magnitude of protection level, the UTPM yields much less Misleading Information than the conventional method.

An advantage of the probabilistic approach is that it directly operates in the position domain and not in the range domain through the H observation matrix as usual. Therefore, no estimation of the UERE is needed, which, in an urban environment, is always a critical point to address.

Despite the interesting capacity and advantage of a probabilistic approach, as just mentioned, the tuning of the method (see Figure 3) and its computation time (3^n LS solutions to combine, n being the number of satellites) limit its practical use so far.

The validation of the integrity indicator introduced here is still going on with several additional datasets

1 already collected in Nantes and Paris. The singula-
2 rities when (and where) misleading integrity infor-
3 mation occurred will deserve particular attention in
4 future investigations.

5 Lastly, but not least, we still aim at reducing the
6 protection level magnitude obtained, in order to
7 match the ITS applications envisaged.

8 ~~AS PROVIDED BY COPYEDITOR~~

9
10 The authors would like to thank the Ministry
11 responsible for transport in France, DGITM (general
12 directorate for infrastructure, transport and the
13 sea), which funded this research work in the frame
14 of the project named Inturb.

15 REFERENCES

16
17
18
19 1. Braasch, M. S., "Multipath Effects," *GPS: Theory and*
20 *Applications, Volume 1*, Parkinson, B. W. and Spilker,
21 J. J., Jr. (Eds.), Progress in Astronautics and
22 Aeronautics Series, AIAA, 1996, pp. 547–568.
23 2. Groves, P. D., Jiang, Z., Wang, L., and M. K. Ziebart,
24 "Intelligent Urban Positioning using Multi-
25 Constellation GNSS with 3D Mapping and NLOS
26 Signal Detection," *Proceedings of the 25th*
27 *International Technical Meeting of the Satellite*
28 *Division of The Institute of Navigation (ION GNSS*
29 *2012)*, Nashville, TN, September 2012, pp. 458–472.
30 3. Wang, L., P. D. Groves, and Ziebart, M. K., "Multi-
31 Constellation GNSS Performance Evaluation for
32 Urban Canyons Using Large Virtual Reality City
33 Models," *Journal of Navigation*, Vol. 65, No. 3, 2012,
34 pp. 459–476.
35 4. Obst, M., Bauer, S., Reisdorf, S., and Wanielik, G.,
36 "Multipath Detection with 3D Digital Maps for Robust
37 Multi-Constellation GNSS/INS Vehicle Localization in
38 Urban Areas," *Proceedings of IEEE/IV*, 2012.
39 5. Groves, P. D. and Jiang, Z., "Height Aiding, C/N_0
40 Weighting and Consistency Checking for GNSS NLOS

41 and Multipath Mitigation in Urban Areas," *Journal of*
42 *Navigation*, Vol. 66, No. 4, 2013, pp. 653–659.
43 6. Miura, S., Hisaka, S., and Kamijo, S., "GPS Multipath
44 Detection and Rectification using 3D Maps,"
45 *Proceedings of IEEE/ITSC* 2013.
46 7. Peyret, F., Bétaille, D., and Mougel, F., "Non-Line-Of-
47 Sight Signal Detection using an on-board 3D Model
48 of Buildings," *Proceedings of the 11th International*
49 *Conference on Telecommunications for Intelligent*
50 *Transport Systems*, 2011.
51 8. Peyraud, S., Bétaille, D., Renault, S., Ortiz, M.,
52 Mougel, F., Meizel, D., and Peyret, F., "About Non-
53 Line-Of-Sight Satellite Detection and Exclusion in a
54 3D Map-Aided Localization Algorithm," *Sensors*,
55 2013, pp. 829–847.
56 9. Bétaille, D., Peyret, F., Ortiz, M., Miquel, S., and
57 Fontenay, L., "A New Modelling based on Urban
58 Trenches to Improve GNSS Positioning Quality of
59 Service in Cities," *IEEE Intelligent Transportation*
60 *Systems Magazine*, Vol. 5, No. 3, 2013, pp. 59–70.
61 10. Ortiz, M., Peyret, F., Renaudin, V., and Bétaille, D.,
62 "From Lab to Road Test," *InsideGNSS*, Sept–Oct
63 2013, pp. 42–60.
64 11. RTCA/DO-229D Appendix J, Minimum Operational
65 Performance Standards for GPS WAAS Airborne
66 Equipment, 2006.
67 12. Leva, J. L., Uijt de Haag, M., and Van Dyke, K.,
68 "Performance of Standalone GPS," Chapter 7, *GPS*
69 *Principles and Applications*, Elliot D. Kaplan, Ed.,
70 Artech House, 1996, pp. 237–320.
71 13. Bétaille, D., "GNSS Accurate Positioning including
72 Satellite Visibility Check in a Multiple Hypotheses 3D
73 Mapping Framework," *Proceedings of ENC GNSS 2013*.
74 14. Bétaille, D., Peyret, F., and Voyer, M., "Applying
75 Standard Digital Map Data in Map-aided, Lane-level
76 GNSS Location," *Journal of Navigation*, Vol. 68, No. 5,
77 2015, pp. 827–847.
78 15. Brown, R. G., "A Baseline GPS RAIM Scheme and a
79 Note on the Equivalence of Three RAIM Methods,"
80 *Navigation*, Vol. 39, No. 3, 1992, pp. 301–316.

Author Query Form

Journal: Navigation


Article: navi_145

Dear Author,

During the copyediting of your paper, the following queries arose. Please respond to these by annotating your proofs with the necessary changes/additions.

- If you intend to annotate your proof electronically, please refer to the E-annotation guidelines.
- If you intend to annotate your proof by means of hard-copy mark-up, please use the standard proofing marks. If manually writing corrections on your proof and returning it by fax, do not write too close to the edge of the paper. Please remember that illegible mark-ups may delay publication.

Whether you opt for hard-copy or electronic annotation of your proofs, we recommend that you provide additional clarification of answers to queries by entering your answers on the query sheet, in addition to the text mark-up.

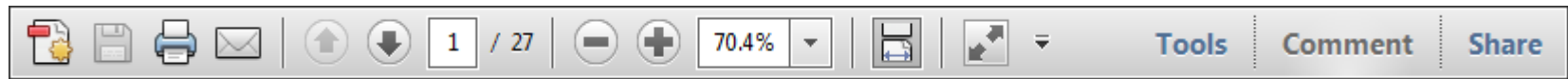
Query No.	Query	Remark
Q1	AUTHOR: Please confirm that given names (red) and surnames/family names (green) have been identified correctly.	
Q2	AUTHOR: Please check that authors' affiliations are correct.	
Q3	AUTHOR: Colors have been mentioned in the text/caption for Figures 1, 3, 5 6–9, 11–12 and 14–17. To ensure that no relevant data would be lost when figures are printed in black and white, please resupply them using symbols instead of colors to differentiate data.	

USING e-ANNOTATION TOOLS FOR ELECTRONIC PROOF CORRECTION

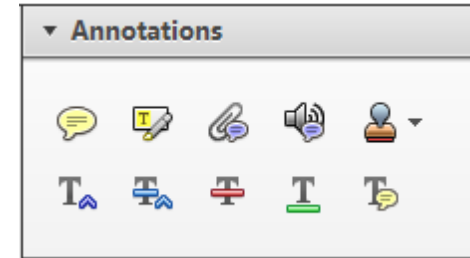
Required software to e-annotate PDFs: Adobe Acrobat Professional or Adobe Reader (version 7.0 or above). (Note that this document uses screenshots from Adobe Reader X)

The latest version of Acrobat Reader can be downloaded for free at: <http://get.adobe.com/uk/reader/>

Once you have Acrobat Reader open on your computer, click on the [Comment](#) tab at the right of the toolbar:



This will open up a panel down the right side of the document. The majority of tools you will use for annotating your proof will be in the [Annotations](#) section, pictured opposite. We've picked out some of these tools below:



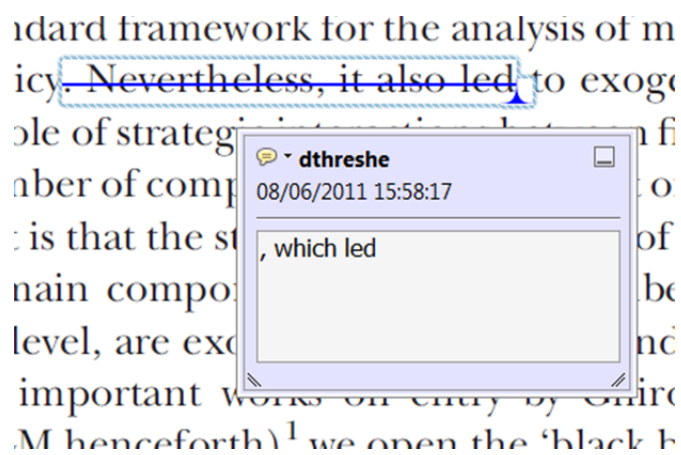
1. Replace (Ins) Tool – for replacing text.



Strikes a line through text and opens up a text box where replacement text can be entered.

How to use it

- Highlight a word or sentence.
- Click on the [Replace \(Ins\)](#) icon in the Annotations section.
- Type the replacement text into the blue box that appears.



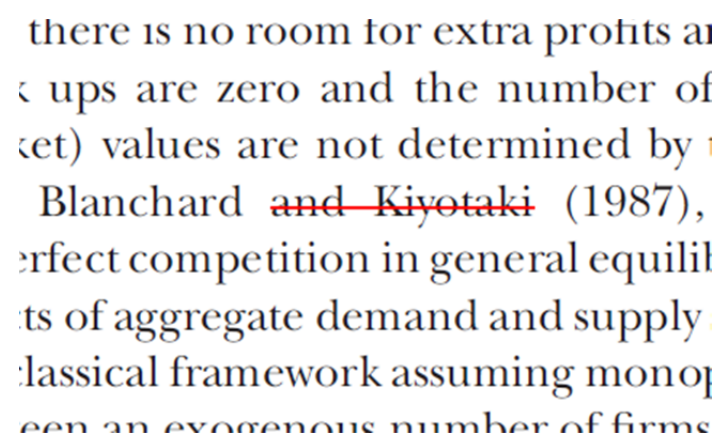
2. Strikethrough (Del) Tool – for deleting text.



Strikes a red line through text that is to be deleted.

How to use it

- Highlight a word or sentence.
- Click on the [Strikethrough \(Del\)](#) icon in the Annotations section.



3. Add note to text Tool – for highlighting a section to be changed to bold or italic.

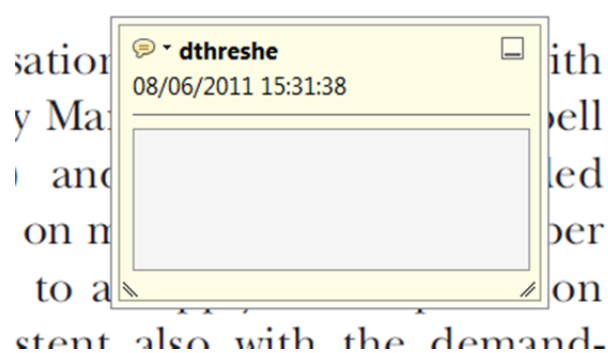


Highlights text in yellow and opens up a text box where comments can be entered.

How to use it

- Highlight the relevant section of text.
- Click on the [Add note to text](#) icon in the Annotations section.
- Type instruction on what should be changed regarding the text into the yellow box that appears.

dynamic responses of mark ups
ent with the **VAR** evidence



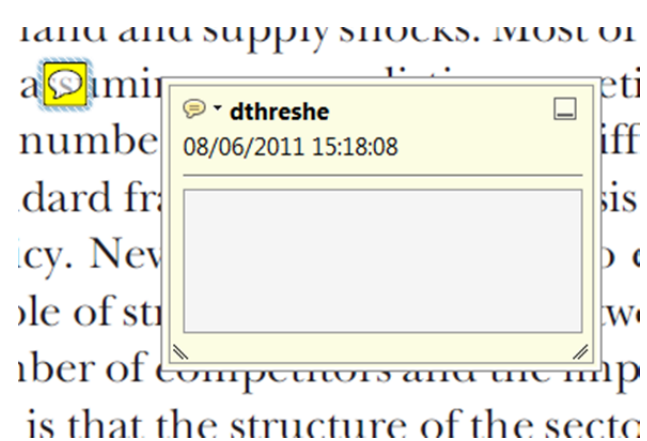
4. Add sticky note Tool – for making notes at specific points in the text.



Marks a point in the proof where a comment needs to be highlighted.

How to use it

- Click on the [Add sticky note](#) icon in the Annotations section.
- Click at the point in the proof where the comment should be inserted.
- Type the comment into the yellow box that appears.



USING e-ANNOTATION TOOLS FOR ELECTRONIC PROOF CORRECTION

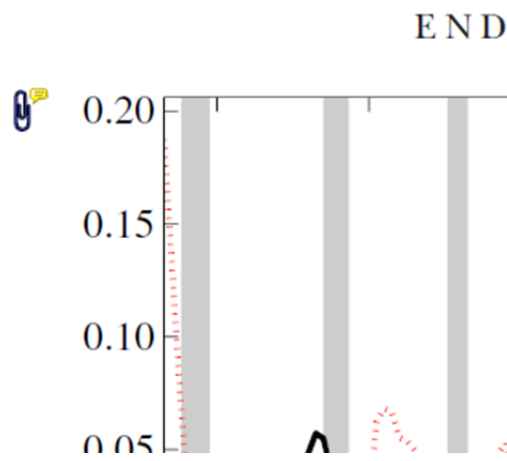
5. Attach File Tool – for inserting large amounts of text or replacement figures.



Inserts an icon linking to the attached file in the appropriate place in the text.

How to use it

- Click on the [Attach File](#) icon in the Annotations section.
- Click on the proof to where you'd like the attached file to be linked.
- Select the file to be attached from your computer or network.
- Select the colour and type of icon that will appear in the proof. Click OK.



6. Add stamp Tool – for approving a proof if no corrections are required.

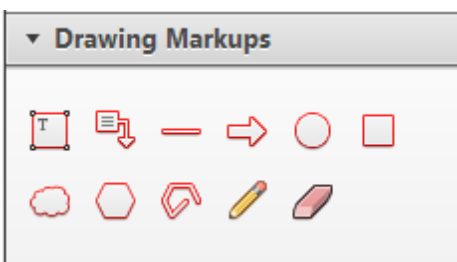


Inserts a selected stamp onto an appropriate place in the proof.

How to use it

- Click on the [Add stamp](#) icon in the Annotations section.
- Select the stamp you want to use. (The [Approved](#) stamp is usually available directly in the menu that appears).
- Click on the proof where you'd like the stamp to appear. (Where a proof is to be approved as it is, this would normally be on the first page).

of the business cycle, starting with the
 on perfect competition, constant return
 production. In this environment goods
 extra profits and the number of firms
 he number of firms is determined by the model. The New-Key
 otaki (1987), has introduced product
 general equilibrium models with nomin
 ed and supply shocks. Most of this literat

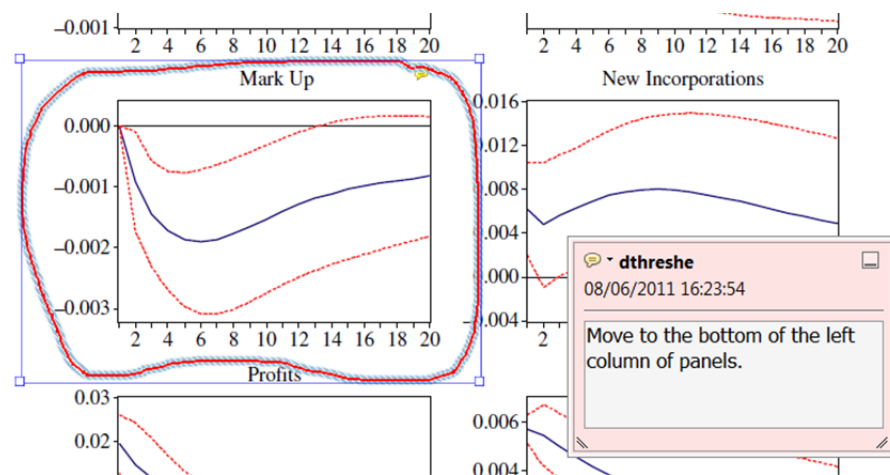


7. Drawing Markups Tools – for drawing shapes, lines and freeform annotations on proofs and commenting on these marks.

Allows shapes, lines and freeform annotations to be drawn on proofs and for comment to be made on these marks..

How to use it

- Click on one of the shapes in the [Drawing Markups](#) section.
- Click on the proof at the relevant point and draw the selected shape with the cursor.
- To add a comment to the drawn shape, move the cursor over the shape until an arrowhead appears.
- Double click on the shape and type any text in the red box that appears.



For further information on how to annotate proofs, click on the [Help](#) menu to reveal a list of further options:

